Frontiers of Information Technology & Electronic Engineering
www.jzus.zju.edu.cn; engineering.cae.cn; www.springerlink.com
ISSN 2095-9184 (print); ISSN 2095-9230 (online)
E-mail: jzus@zju.edu.cn

Supplementary materials for

Yu GAN, Lin LIU, Jian BAI, Hongfu MENG, 2024. An orbital angular momentum multiplexing communication system at 28 GHz with an active uniform circular array. *Front Inform Technol Electron Eng*, 25(12):1759-1768. https://doi.org/10.1631/FITEE.2400376

1 Supplement to the analysis of non-line-of-sight (NLoS) conditions

In our experiment, while confined to the limitations of a non-ideal microwave anechoic chamber, the primary NLoS influence stems from ground multipath effects. This phenomenon is intrinsically linked to the nature of OAM and its interaction with the environment. Specifically, ground multipath effects in the context of OAM can be attributed to the two following primary factors:

1. Diffusion Effect of Traditional OAM: The spiral phase front inherent to OAM beams causes them to spread out as they propagate, leading to a broader beamwidth and increased susceptibility to multipath interference. This effect is exacerbated in NLoS scenarios where reflections from the ground can cause significant distortions.

2. Filtering Effect at the OAM Receiver: The receiver's ability to decode the OAM state is affected by the phase distortions introduced by ground reflections. These distortions can alter the spiral phase pattern, impacting the receiver's filtering efficiency and potentially leading to cross-talk between different OAM modes.

Fig. S1 shows the concept of the multipath effects of an OAM beam caused by the specular reflection from a reflector parallel to the link. An OAM channel with an OAM number of $\ell 1$ is transmitted along the link. At the receiver end, the receiver has an OAM number of $\ell 2$. Ideally, power can be recovered only when $\ell 1=-\ell 2$, owing to the orthogonality of OAM beams in a line-of-sight link. However, the orthogonality no longer holds when the receiver receives the reflected beam.

As shown in Fig. S2, a reflector is placed at a distance h away from the beam center. Assuming that the reflector has a reflection coefficient of 100%, the reflected beam can be observed as an OAM beam from an imaging antenna Tx and an imaging transmitter with an OAM number of $-\ell 1$ (reflection changes the sign of the OAM value). Therefore, the receiver will receive an OAM beam with an OAM number of $\ell 1$ from the original link as well as a reflected beam with an OAM number of $-\ell 1$ from an offset link, which is placed at a distance of 2 h.

The orthogonality of the OAM beams depends on the spiral wavefront. Reflection is likely to distort the wavefront phase and induce both intra-channel and inter-channel crosstalk. Further, reflection causes the distortion of the OAM beam's intensity, giving rise to both intra-channel and inter-channel crosstalk. To illustrate this phenomenon, we use an OAM beam with $\ell 1=+3$ as an example. In Fig. S2, the left-hand-side column shows the intensity, phase, and OAM spectrum of the OAM beam in the direct path. The entire power is in the OAM state of $\ell 1=+3$.

The middle column shows the reflected OAM beam. The reflected OAM beam exhibits an OAM number of $\ell 1'=-3$, and it is offset to the direct link. As a result, when the reflected OAM beam is decomposed with respect to the OAM basis along the direct path axis, power diverges onto a wide range of OAM states, leading to intra-channel crosstalk with an OAM channel with $\ell 1=+3$ and inter-channel crosstalk with the other OAM channels with $\ell 1\neq+3$. The column on the right side of Fig. S2 shows the actual beam at the receiver, which is the superposition of the direct and reflected beams. The intensity exhibits a fringing pattern owing to the

interference between the direct and reflected beams. The wavefront phase is also distorted owing to the multi-path effect. The power of the actual received OAM with $\ell 1=+3$ differs from that of the directed path because of the intra-channel crosstalk from the reflected beam, and the received power of the other OAM beams with values of $\ell 1 \neq +3$ is nothing but the inter-channel crosstalk from the reflected beam.

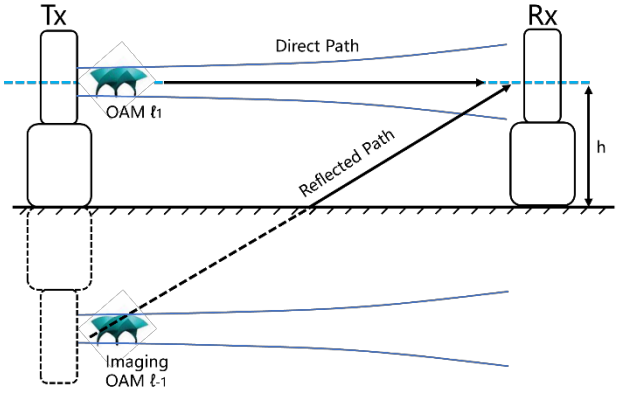

Fig. S1 Multipath effects of an OAM channel caused by specular reflection from a parallel ideal reflector

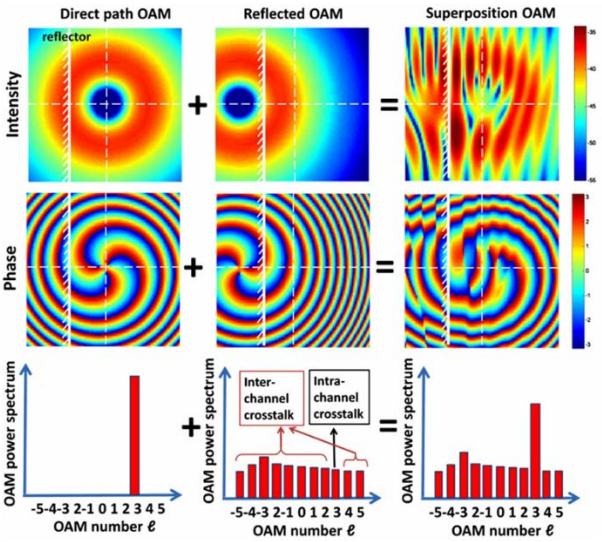

Fig. S2 Simulation results showing the intensity, phase, and OAM spectrum of the direct path OAM beam, reflected path OAM beam, and the actual beam at the receiver

To mitigate these effects, we employed two key strategies:

1 Increasing Antenna Height: by elevating the antennas above the ground, we reduced the strength of ground reflections relative to the direct path, thereby minimizing their interfering impact on the OAM beam.

2 Utilizing Lower-Order OAM Modes: higher-order OAM modes exhibit a wider diffusion angle, causing their energy to disperse more rapidly. By focusing on lower-order modes, we were able to maintain a more concentrated beam, reducing the susceptibility to multipath interference.

To further assess the impact of NLoS conditions on our communication performance, we analyzed the near-field amplitude and phase data collected during the experiments. This analysis allowed us to estimate the energy distribution of the background OAM spectrum within the test environment. By comparing the energy amplitudes of the primary OAM mode with those of the surrounding modes, we gained insight into the level of cross-interference.

As illustrated in Fig. 6 of the manuscript, our calculations reveal that the energy from neighboring modes contributes to less than 15 dB of cross-interference with the primary mode. This finding indicates that the NLoS conditions had a minimal impact on our measurement results, validating our approach to mitigating multipath effects and ensuring the robustness of our communication performance.

In summary, while the NLoS conditions posed a potential challenge to our experiment, we addressed this using a combination of theoretical analysis and practical measures. By understanding the specific mechanisms of ground multipath effects on OAM and implementing strategies to minimize these impacts, we were able to demonstrate that the NLoS scenarios had only a minor influence on our measurement outcomes.

2 Supplement to the analysis of non-uniform phase calibration

We concluded that the impact of phase errors within ±10 degrees has a relatively minor effect on the overall OAM mode purity. To further elaborate on this point and provide additional evidence, we conducted a MATLAB simulation to compare the phase distribution of the calibrated +1 OAM mode with the ideal perfect phase distribution. We employed a near-field integral simulation method for this purpose and calculated the OAM spectra

In the simulation, we modeled the phase distribution of the calibrated +1 OAM mode, incorporating the phase errors within the stated tolerance. We then compared this distribution with the ideal phase distribution, which exhibits a perfectly uniform phase shift across the antenna elements. By utilizing the near-field integral method, we computed the electric field distributions and subsequently derived the OAM spectra for both the calibrated and ideal cases.

The simulation results revealed that, despite the imperfections in the calibrated phase distribution, the OAM mode purity remained high, with minimal leakage into other OAM modes. This finding supports our earlier assessment that phase errors within ±10 degrees have a limited impact on the mode purity.

We believe that these simulations provide a robust justification for our approach and demonstrate that the phase calibration imperfections, while present, do not significantly degrade the performance of our OAM multiplexing system. We are committed to ensuring the accuracy and reliability of our results and will continue to explore methods to further minimize phase errors in future work.

Table S1 Comparison of calibrated phase distribution with ideal phase distribution

	ℓ	Forward transmission coefficient (degree)							
		CH1	CH2	CH3	CH4	CH5	CH6	CH7	CH8
After calibrating	+1	1	47	87	139	−173	−129	−85	−48
Ideal distribution	+1	0	45	90	135	−180	−135	−90	−45

* Taken from data captured by Vector Network Analyzer at 28 GHz

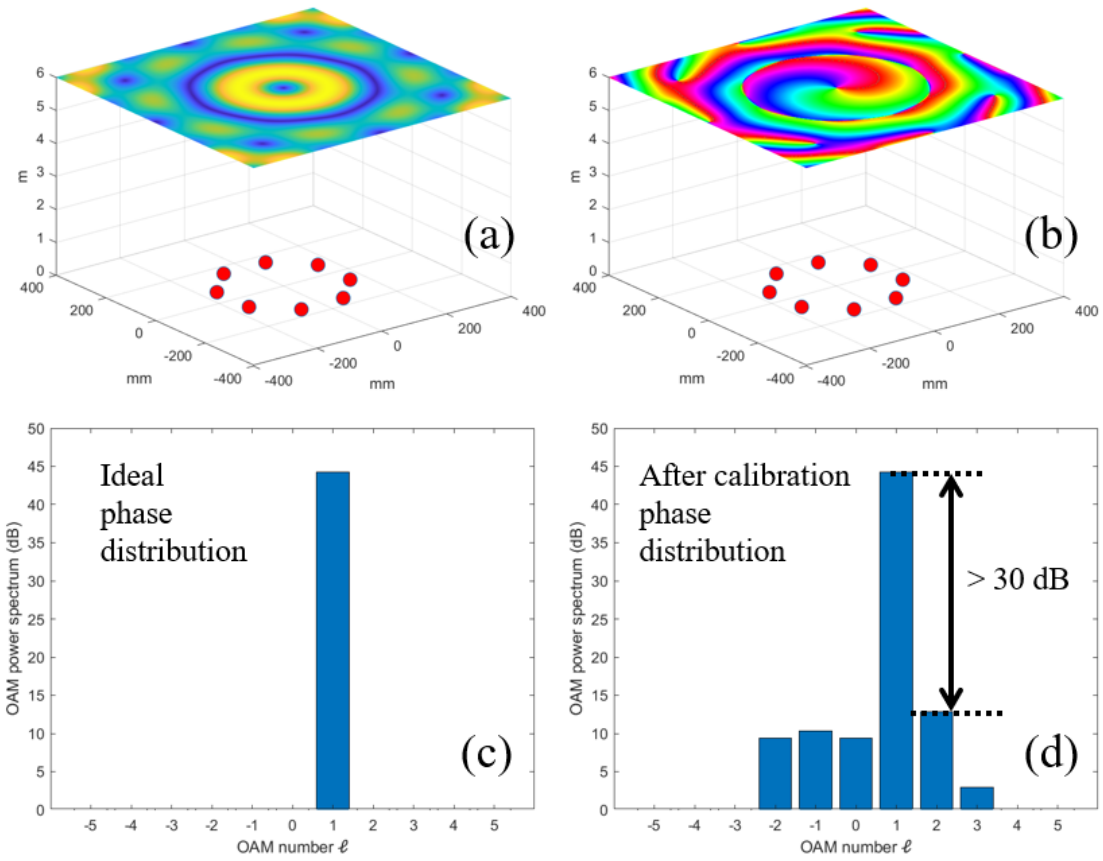

Fig. S3 Analysis of OAM interference between ideal phase distribution and actual phase distribution. Near-field electromagnetic field simulation as shown in (a) and (b), the calculated ideal phase distribution OAM spectrum (c), and the phase distribution OAM spectrum after calibration (d)

3 Supplement to the measurement of near field with different distance

Fig. S4 shows the measured results of the first-order and second-order OAM beams. The light spot of the OAM beam around the center disperses along the diffusion angle, which ranges from 1.8 deg to 2.2 deg.

The OAM modal intensity distributions appear imperfect. A closer inspection of the near-field measurements at two meters and four meters (Fig. S4) reveals that the amplitude distributions are relatively more uniform compared to the six-meter distance. This discrepancy can be attributed to several factors, including variations in the output power of different channels of the T/R chip and the bending of coaxial lines.

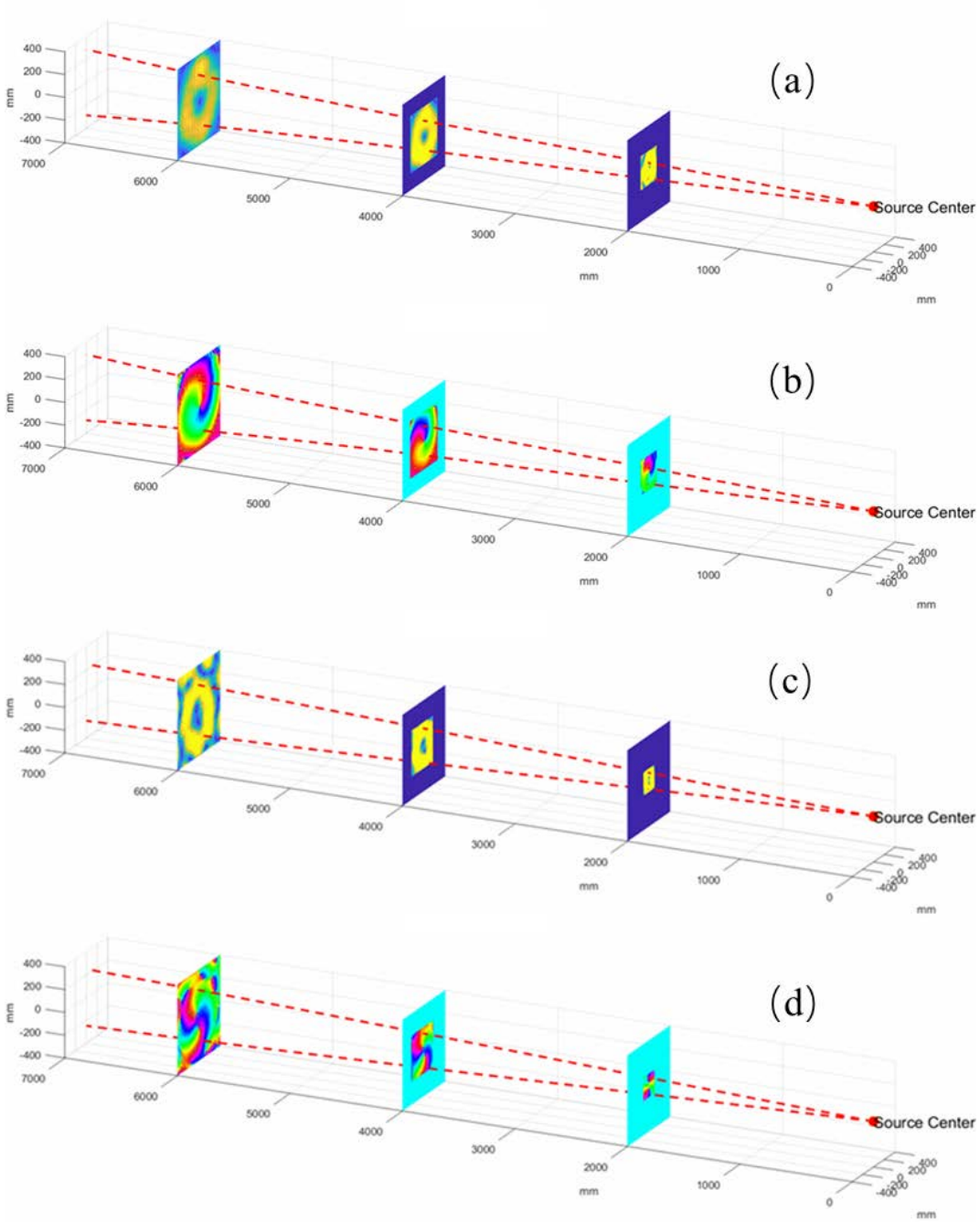

Fig. S4 Measured electric field intensity and measured phase distribution of different OAM modes. Measured electric field intensity at cross-sections of 2 m, 4 m, and 6 m away from the Tx antenna with OAM mode +1(a), −2(c) and measured phase distribution of OAM mode +1(b), −2(d)